Quarter-wave plate metasurfaces on electromagnetically thin polyimide substrates

L. Maiolo,[1] A. Ferraro,[1] F. Maita,[1] R. Beccherelli,[1] E. E. Kriezis,[2] T. V. Yioultsis,[2] and D. C. Zografopoulos[1, a)]

[1)] *Consiglio Nazionale delle Ricerche, Istituto per la Microelettronica e Microsistemi (CNR-IMM), 00133 Rome, Italy*

[2)] *School of Electrical and Computer Engineering, Aristotle University of Thessaloniki (AUTH), 54124 Thessaloniki, Greece*

(Dated: 18 November 2019)

We experimentally demonstrate that electromagnetically thin polyimide substrates can mitigate substrate-induced detrimental effects to the performance of metallic metasurfaces. A planar quarter-wave plate for the microwave K-band is fabricated on a polyimide substrate of deeply subwavelength thickness by means of standard photolithography. By properly selecting the combination of the polyimide thickness and the aluminum layer thickness of the metasurface, conversion from linear to circular polarization is achieved at the design frequency. The proposed approach is generic and it can be applied to the fabrication of mechanically robust, flexible metallic metasurfaces, which are primarily designed to work in free-standing configuration.

Metasurfaces are two-dimensional periodic arrays of subwavelength scattering elements that offer unprecedented functionalities in terms of manipulating the propagation of electromagnetic waves[1]. By harnessing the resonances supported by the individual scatterers, as well as their collective oscillations, both the in-plane spatial phase profile and the power spectral response of metasurfaces can be accurately controlled, while maintaining deeply subwavelength overall thickness. Such properties can be directly exploited in compact and planar devices for beam steering, lensing, polarization control, and filtering[2], to name but a few of the enabled applications.

The constituent elements of a metasurface can be metallic or dielectric, the latter gaining more popularity at infrared or visible wavelengths, as they are free from ohmic losses. However, at microwave, millimeter-wave and up to terahertz (THz) frequencies, where most metals are good conductors, metallic metasurfaces are the standard choice, as they can be readily fabricated by well-established techniques, ranging from printed circuit board (PCB) etching and direct laser ablation to photolithography. The latter, in particular, becomes more relevant as the operation frequency shifts towards the THz spectrum, where the subwavelength dimensions of the metallic elements composing the metasurface shrink and micrometric resolution is often needed.

Metasurfaces are usually patterned on a dielectric substrate, preferably low-loss. Free-standing metallic metasurfaces can also be fabricated, for instance via electroplating[3], however they are fragile and need some mechanical support, while their fabrication is generally cumbersome and cannot be easily scaled to higher frequencies. More important, they are limited to structures with interconnected metallic networks, which rules out a large number of designs, such as those that employ metallic patches or split-rings.

[a)] Electronic mail: dimitrios.zografopoulos@artov.imm.cnr.it

The presence of the dielectric substrate naturally induces a spectral shift of the metasurface resonances, although it may not necessarily affect the overall performance of the device, as in the case of cross-shaped bandpass frequency-selective surface (FSS) filters[4]. However, such spectral shifts depend largely on the resonator type of the metasurface. As a characteristic example, the substrate breaks the symmetric response of complementary structures dictated by Babinet's principle[5], thus rendering this handy design tool ineffective. What's more, in certain cases the substrate's effect can be severely detrimental, as in the case of metasurfaces whose operation relies on polarization-dependent phase shifts[6] or very strong resonances, which are damped by the absorption losses introduced by the dielectric substrate[7,8].

In this work, we experimentally present an approach based on the use of electromagnetically ultrathin polyimide substrates, which mitigate the aforementioned negative effects, while still providing mechanical robustness and flexibility to metallic metasurfaces. Polyimides have been long used in microwave technology as dielectric spacers, such as in microstrip lines[9], and more recently in microwave or THz metamaterials, such as for absorption[10], diffuse scattering[11], cloaking[12], and polarization conversion[13], including multilayer stacks[14]. They have also been employed as substrates for THz filters in FSS[15] or guided-mode resonant configurations[16] in order to provide mechanical support and waveguiding in the dielectric layer, respectively. However, such functions are not relevant to the paradigm introduced in this work and, in principle, they can be also achieved with similar or better performance by using other lower-loss polymeric substrates[4,17]

As a proof-of-concept, we investigate an ultrathin quarter-wave plate metasurface (QWPM) fabricated by standard photolithography and designed for operation in the IEEE K-band ($18 - 27$ GHz), which is relevant for high-frequency 5G wireless communications. The thickness of the polyimide substrate is extremely subwavelength, thus introducing a very weak electromagnetic

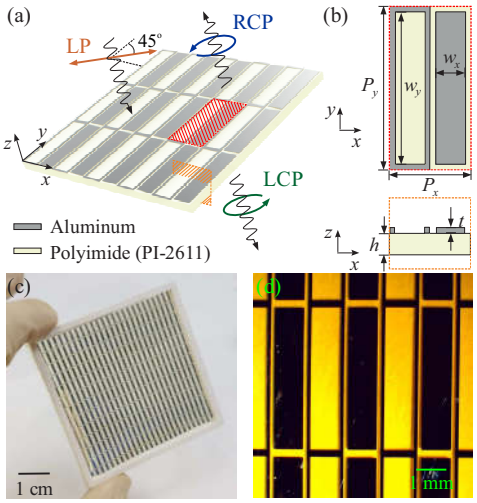

FIG. 1. (a) Schematic 3D layout of the investigated metasurface that acts as an ultrathin quarter-wave plate at the operation frequency: a linearly polarized (LP) impinging planewave splits in two beams of equal intensity one of which is left circularly polarized (LCP) and the other right circularly polarized (RCP). (b) Cross-sections of the device and definition of the geometrical parameters of the structure. (c) Photo of the fabricated sample mounted on a 3D-printed plastic frame. (d) Micrograph taken under stereomicroscope in reflection mode showing the geometrical features of the metasurface.

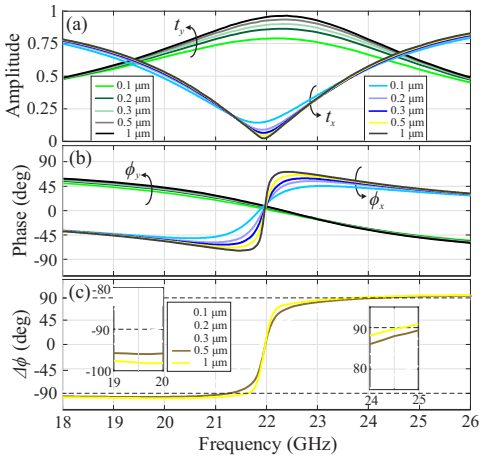

FIG. 2. Electromagnetic response of the investigated quarter-wave plate metasurface for a polyimide substrate thickness of $h = 8$ μm and five values of the aluminum layer thickness from $t = 0.1$ μm to $t = 1$ μm. (a) Amplitude and (b) relative phase of the field transmission coefficients for the two orthogonal polarizations of the impinging wave. (c) Phase difference, defined as $\Delta\phi = \phi_x - \phi_y$. The insets zoom on the spectral windows intended for linear-to-circular polarization conversion.

effect while providing both mechanical robustness and flexibility. The layout of the metasurface is shown in Fig. 1(a) and it is based on a self-complementary structure that acts as a compact quarter-wave plate. Self-complementary metasurfaces are ideal structures for the realization of free-space quarter-wave plates as they feature a key electromagnetic property, i.e., the field transmission and reflection coefficients for the two orthogonal polarizations are phase-shifted by 90 degrees, for the ideal case of a suspended, infinitesimally thin, perfect electric conductor screen. Such property is a direct consequence of electromagnetic energy conservation, the continuity of the tangential components of the electric field at the surface, Babinet's principle, and the invariability of the field transmission and reflection coefficients between the original and complementary structure[6].

In principle, any self-complementary metasurface can act as a QWPM. We have opted for the 2D array of rectangular patches and holes depicted in Fig. 1 since in the systematic study of Ref. [6] it was found to provide some comparative advantages, namely relatively large operation bandwidth and small element size, which enables safe operation away from the diffraction regime, even for oblique incidence. Although demonstrated experimentally at lower frequencies, such a waveplate's performance deviated significantly from the ideal behaviour mainly due to the presence of a standard microwave dielectric substrate[6] with a thickness of 500 μm. Here, we demonstrate that such effects can be suppressed by judiciously selecting the thicknesses of the polyimide substrate and of the aluminum layer on which the metasurface is patterned. Aluminum was selected as the metasurface metal since it provides certain advantages from the point of view of the employed fabrication, compared to, e.g., copper: i) it has a lower melting point and thus induces significantly less mechanical stress on the polyimide substrate, ii) it does not need extra fabrication steps to promote its adhesion to the polyimide, and iii) it leads to uniform films with low surface roughness.

Figure 1(b) shows the metasurface unit cell, whose pitch along the x- and y-axis is $P_x = 2.5$ mm and $P_y = 5$ mm, respectively. For these pitch values the periodic metasurface remains non-diffractive up to 60 GHz for normal incidence, which provides ample margin of operation in the targeted frequency band. The unit cell is subdivided in two parts with complementary structures. The central rectangular patch in each part has dimensions equal to $w_x = 1$ mm and $w_y = 4.75$ mm. The thickness of the polyimide substrate is h, whereas t is the thickness of the aluminum layer. The metasurface prop-

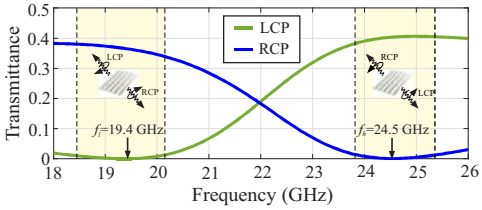

FIG. 3. Power transmittance of the LCP and RCP waves for a LP normally impinging planewave polarized at 45°. The yellow zones mark the 3−dB axial ratio bandwidth around the working frequencies $f_l = 19.4$ GHz and $f_h = 24.5$ GHz.

erties were theoretically investigated by full-wave simulations based on the finite-element method, implemented in the commercial software COMSOL Multiphysics®. The structure was studied for the case of normal planewave incidence by properly applying periodic boundary conditions at the lateral walls defining the unit cell. The conductivity of aluminum considered in the simulations was $\sigma_m = 3.77 \times 10^7$ S/m and the complex relative dielectric permittivity of the polyimide substrate[9,18] was $\varepsilon_s = 3.3(1 - j0.006)$.

Figure 2 shows the full electromagnetic response of a QWPM with $h = 8$ µm and five values of the aluminum layer thickness t ranging from 0.1 to 1 µm. As some of the considered thickness values are smaller than the skin depth of aluminum in the investigated frequency range, equal to 520 nm at 25 GHz, aluminum was modeled as a bulk material with its entire volume meshed in the finite-element simulations. The amplitude and relative phase of the field transmission coefficient were calculated for the two orthogonal polarizations of a normally impinging planewave: $t_{x,y} = |S_{21}^{x,y}|$, $\phi_{x,y} = \angle S_{21}^{x,y} - \angle S_{21}^{\text{ref}}$, where $\angle S_{21}^{\text{ref}}$ is the reference phase corresponding to propagation in free space, and $\Delta\phi = \phi_x - \phi_y$.

In all cases examined there are two frequencies, $f_l \simeq 19.5$ GHz and $f_h \simeq 24.5$ GHz, where the amplitudes for the two polarizations match ($t_x = t_y$, as shown in Fig. 2(a)), whereas their relative phase difference equals approximately −90° and 90°, respectively (see Fig. 2(c)). Hence, for a planewave linearly polarized at 45° the metasurface acts as a quarter-wave plate at f_l and f_h, the only difference being the handedness of the resulting circularly polarized (CP) waves. In the ideal lossless case described by the conditions $t_x = t_y = 1/\sqrt{2}$ and $\Delta\phi = \pm 90°$, namely in the absence of substrate and considering zero-thickness perfect electric conductor patches and frames for the metallic parts, the impinging wave splits in two circularly polarized waves of equal amplitude, one of which is transmitted and the other reflected, as schematically shown in Fig. 1(a). However, a realistic QWPM is expected to deviate from the optimal performance owing to an additional polarization-dependent phase shift induced by the substrate and to the finite thickness and conductivity of the aluminum parts, as thoroughly discussed in Ref. [6]. The presence of the substrate induces also a relative frequency shift Δf_r between the resonant frequencies f_r^x and f_r^y for $x-$ and $y-$polarized planewaves. Such shift lifts the symmetric spectral response of the metasurface, such that the field amplitudes $|t_x| = |t_y| = |t_{x,y}|$ at the two working frequencies f_l and f_h are not the same.

TABLE I. Key operation and performance parameters of the investigated QWPM.

f_l	19.4 GHz	$\lvert t_{x,y}(f_l)\rvert$	0.603	Excess IL (f_l)	1.39 dB
f_h	24.5 GHz	$\lvert t_{x,y}(f_h)\rvert$	0.638	Excess IL (f_h)	0.9 dB
f_r^x	21.95 GHz	$\Delta\phi(f_l)$	−91°	ARBW/f_l	8.76%
f_r^y	22.2 GHz	$\Delta\phi(f_h)$	86°	ARBW/f_h	6.29%

Slight deviations in the amplitude coefficients for the transmitted field ($t_x \neq t_y$) can be compensating by rotating the polarization axis of the LP planewave or, equivalently, the QWPM. In such a way, the ratio of the electric field components of the impinging wave can be adjusted so that the amplitudes of the transmitted wave components are equal[19]. On the contrary, the phase difference depends on the structural parameters and it cannot be *a posteriori* controlled. Nevertheless, Fig. 2(c) demonstrates that a way to accurately adjust the phase difference at the desired value is by properly selecting the thickness of the aluminum layer in the design stage of the metasurface. The Al thickness can be accurately controlled during the employed fabrication process down to values significantly lower than the skin depth, which is not an option in the case of free-standing or standard PCB metasurfaces. For the investigated structure, it was found that for $t = 200$ nm the phase difference at f_l becomes $\Delta\phi = -91°$, thus allowing for almost perfect LP to CP conversion. Similarly, in case operation at f_h is targeted, a thickness of $t = 1$ µm was found to yield the best performance. The analysis demonstrated that the metal layer thickness, which is usually considered to be higher than the skin depth, provides an additional degree of freedom for the fine-tuning of the properties of metallic metasurfaces.

The set of values $h = 8$ µm and $t = 200$ nm was selected for the demonstration of the QWPM. According to Fig. 2, the working frequencies of the QWPM are $f_l = 19.4$ GHz and $f_h = 24.5$ GHz, at which $|t_{x,y}|$ obtains the value of 0.603 and 0.638, respectively. The corresponding phase difference at the two frequencies are $\Delta\phi(f_l) = -91°$ and $\Delta\phi(f_h) = 86°$. The resonant frequencies for the two polarizations differ by 0.25 GHz, which is approximately 1% of their average frequency $f_m = (f_r^x + f_r^y)/2$, where $f_r^x = 21.95$ GHz and $f_r^y = 22.2$ GHz. We further define the 3-dB axial ratio bandwidth (ARBW) as the spectral window for which $1 \leq \max(|t_x|/|t_y|, |t_y|/|t_x|) \leq \sqrt{2}$, which is a commonly adopted metric for the estimation of the operational bandwidth of a quarter-wave plate[6]. Under such definition, the ARBW around f_l and f_h for the investi-

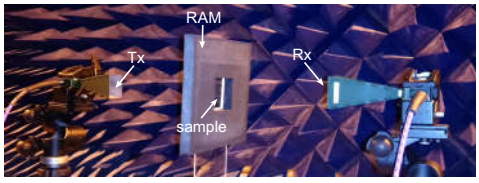

FIG. 4. Photograph of the experimental setup, showing the transmit (Tx) and receive (Rx) horn antennas and the sample, attached on its placeholder, i.e., a slab made of radar absorbing material (RAM) with a square opening. The complete experimental setup is accommodated within an anechoic chamber.

gated QWPM is 1.7 and 1.54 GHz, respectively, which correspond to relative bandwidths ARBW/$f_{l,h}$ equal to 8.76% and 6.29%.

Based on the values of $|t_{x,y}|$, the power transmittance coefficient for the converted RCP and LCP waves at f_l and f_h, respectively, is calculated as $P_{\mathrm{RCP}} = |t_{x,y}(f_l)|^2 = 0.364$ and $P_{\mathrm{LCP}} = |t_{x,y}(f_h)|^2 = 0.407$. This is directly demonstrated in the results Figure 3, which shows the power transmittance coefficients for RCP and LCP waves for a normally impinging LP planewave polarized at 45°, as well as the respective ARBW. Pure conversion without residues of the unwanted circular polarization is achieved at the two working frequencies. The reported transmittance values correspond to insertion losses (IL) of 4.39 dB and 3.9 dB at f_l and f_h, respectively. However, the minimum expected IL, which corresponds to the case of an ideal metasurface are 3 dB, as the QWPM splits the LP impinging wave in two equal parts, one of which is reflected with the opposite CP of the transmitted wave. Hence, the excess IL of the device at f_l and f_h are 0.9 dB and 1.39 dB, respectively. These excess IL were found to stem almost exclusively from ohmic losses in the metallic parts and a small contribution, less than 0.2 dB, from the deviation of the reflected wave power from the reference value of 3 dB. Importantly, the power lost in the dielectric substrate was less than 0.5% in both operation bandwidths. Table 1 summarizes all the performance parameters and metrics of the investigated QWPM.

The manufacturing procedure of the QWPM consisted of five main fabrication steps: i) a 8 µm-thick polyimide (PI-2611, HD MicroSystems) layer was deposited onto a 3″ silicon substrate, cleaned with a buffered HF solution, by spin-coating and cured in vacuum oven at 250 °C. ii) An Al film of thickness $t = 200$ nm was evaporated on the cured polyimide, after a reactive ion etching treatment of the polyimide surface in order to promote adhesion. iii) A film with thickness 1.3 ± 0.1 µm of the photoresist S1813 (Shipley) was spin-coated at 4000 rpm for 60 sec and then cured at a temperature of 115 °C for 120 sec. iv) The photolithography of the metasurface pattern was carried out using a Karl Suss MA150 mask aligner ($\lambda = 365$ nm, $I = 60$ mW/cm^2). The sample was immersed in the developer MF319 for 50 sec, rinsed with DI water, dried with nitrogen and cured at 120 °C for 5 min. The aluminum layer was wet-etched and the residual photoresist was removed with acetone and washed with isopropanol. v) Finally, the polyimide layer was peeled off the Si substrate wafer, cut into a square area of 5×5 cm^2, and mounted on a 3D-printed plastic frame, as shown in Fig. 1(c). A zoomed photo of a few metasurface unit cells taken under stereomicroscope in reflection mode is shown in Fig. 1(d). The inspection of the fabricated sample revealed a small variation of its dimensions with respect to the nominal values by 5 µm due to a slight overetching of the photolithographic mask. This effect was included in the numerical analysis that follows.

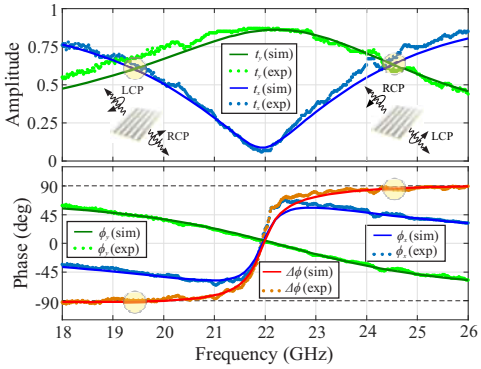

FIG. 5. Comparison of the experimentally measured properties of the investigated QWPM with those theoretically simulated by means of the finite-element method. The yellow spots indicate the frequencies where linear to circular polarization conversion takes place.

The experimental evaluation was conducted in an anechoic chamber, using a pair of standard gain 20 dBi, K-band (17.6-26.7 GHz) horn antennas (FLANN Microwave 20240) and a Vector Network Analyzer (Anritsu 37397D). A view of the measurement setup is shown in Fig. 4, with the sample placed in perfect alignment between the transmit and receive antennas. The sample is mounted on a lightweight plastic frame as in Fig. 1(c), which is subsequently attached to a square opening, cut on a slab made of radar absorbing material (RAM), in order to eliminate spurious diffraction effects. Transmission measurements, for both polarizations, have been taken with response calibration, using as reference the two-antenna link in the absence of the sample.

A direct comparison between the experimentally measured QWPM electromagnetic response with that theoretically simulated is provided in Fig. 5. Excellent agreement is observed, particularly as far as the phase difference $\Delta\phi$ is concerned, which is the most critical property that determines the quality of polarization con-

version. The measured phase difference at $f_l = 19.4$ GHz was $-89°$ (viz. the theoretical value of $-91°$), while at $f_h = 24.5$ GHz the measured value of 86° matched the one theoretically calculated.

Overall, the thin polyimide substrate was demonstrated to provide mechanical support and flexibility to the QWPM without compromising its performance, which was the main goal of this study. The substrate thickness of 8 μm was selected as a reasonable trade-off between the necessity for an electromagnetically thin substrate and adequate robustness and fabrication ease of the device. Thinner substrates of the same material (PI-2600 series by HD MicroSystems™) can be spin-coated down to values as low as 1 μm to eliminate the minor residual substrate effects or to allow scaling of the device to higher frequencies.

In addition, the employed fabrication technique, namely the photolithographic patterning of an metallic layer evaporated on the polyimide substrate, was found to provide an extra degree of freedom for the fine-tuning of the metasurface response, that is the thickness of its metallic layer. It is stressed that the proposed approach is not limited to components for polarization conversion or self-complementary structures and it can be applied to any metasurface that suffers from substrate-induced performance deterioration, such as strongly resonant metasurfaces with high electromagnetic near-field confinement[8].

This research has been co-financed by the European Union and Greek national funds through the Operational Program Competitiveness, Entrepreneurship and Innovation, under the call RESEARCH CREATE INNOVATE (project code: T1EDK-02784). D.C.Z acknowledges the support by the European Union COST Actions CA16220 "European Network for High Performance Integrated Microwave Photonics" and CA18223 "Future communications with higher-symmetric engineered artificial materials".

[1] H.-T. Chen, A. J. Taylor, and N. Yu, Rep. Prog. Phys. **79**, 076401 (2016).
[2] F. Ding, A. Pors, and S. I. Bozhevolnyi, Rep. Prog. Phys. **81**, 026401 (2017).
[3] F. Baumann, W. A. Bailey, A. Naweed, W. D. Goodhue, and A. J. Gatesman, Opt. Lett. **28**, 938 (2003).
[4] A. Ferraro, D. C. Zografopoulos, R. Caputo, and R. Beccherelli, IEEE J. Sel. Topics Quantum Electron. **23**, 8501308 (2017).
[5] F. Falcone, T. Lopetegi, M. A. G. Laso, J. D. Baena, J. Bonache, M. Beruete, R. Marqués, F. Martín, and M. Sorolla, Phys. Rev. Lett. **93**, 197401 (2004).
[6] J. D. Baena, J. P. del Risco, A. P. Slobozhanyuk, S. B. Glybovski, and P. A. Belov, Phys. Rev. B **92**, 245413 (2015).
[7] I. A. I. Al-Naib, C. Jansen, and M. Koch, Appl. Phys. Lett. **94**, 153505 (2009).
[8] A. A. Basharin, V. Chuguevsky, N. Volsky, M. Kafesaki, and E. N. Economou, Phys. Rev. B **95**, 035104 (2017).
[9] G. Ponchak and A. Downey, IEEE Trans. Compon., Packag., Manuf. Technol. B **21**, 171 (1998).
[10] M. D. Astorino, R. Fastampa, F. Frezza, L. Maiolo, M. Marrani, M. Missori, M. Muzi, N. Tedeschi, and A. Veroli, Scientific Reports **8**, 1985 (2018).
[11] Y. Zhang, L. Liang, J. Yang, Y. Feng, B. Zhu, J. Zhao, T. Jiang, B. Jin, and W. Liu, Sci. Rep. **6**, 26875 (2016).
[12] M. Wei, Q. Yang, X. Zhang, Y. Li, J. Gu, J. Han, and W. Zhang, Opt. Express **25**, 15635 (2017).
[13] N. K. Grady, J. E. Heyes, D. R. Chowdhury, Y. Zeng, M. T. Reiten, A. K. Azad, A. J. Taylor, D. A. R. Dalvit, and H.-T. Chen, Science **340**, 1304 (2013).
[14] S. Liu, A. Noor, L. L. Du, L. Zhang, Q. Xu, K. Luan, T. Q. Wang, Z. Tian, W. X. Tang, J. G. Han, W. L. Zhang, X. Y. Zhou, Q. Cheng, and T. J. Cui, ACS Photonics **3**, 1968 (2016).
[15] D. Zhai, Y. Yang, Z. Geng, B. Cui, and R. Zhao, IEEE Trans. THz Sci. Technol. **8**, 719 (2018).
[16] S. Song, F. Sun, Q. Chen, and Y. Zhang, IEEE Trans. THz Sci. Technol. , 131 (2014).
[17] A. Ferraro, D. C. Zografopoulos, R. Caputo, and R. Beccherelli, Sci. Rep. **8**, 17272 (2018).
[18] Q. G. Kang, *Characterization of vertical interconnects in 3-D monolithic microwave integrated circuits (3-D MMIC)*, Ph.D. thesis, University of Cincinnati (2003).
[19] B. Vasić, D. C. Zografopoulos, G. Isić, R. Beccherelli, and R. Gajić, Nanotechnology **28**, 124002 (2017).